UCSF
UC San Francisco Previously Published Works

Title

Neurophysiological signatures in Alzheimer's disease are distinctly associated with TAU, amyloid-β accumulation, and cognitive decline

Permalink

https://escholarship.org/uc/item/51d5k1rg

Journal

Science Translational Medicine, 12(534)

ISSN

1946-6234

Authors

Ranasinghe, Kamalini G
Cha, Jungho
Iaccarino, Leonardo
et al.

Publication Date

2020-03-11

DOI

10.1126/scitranslmed.aaz4069

Peer reviewed

eScholarship.org Powered by the California Digital Library
University of California

Author Manuscript

Author Manuscript

Author Manuscript

Author Manuscript

HHS Public Access

Author manuscript

Sci Transl Med. Author manuscript; available in PMC 2020 April 11.

Published in final edited form as:

Sci Transl Med. 2020 March 11; 12(534): . doi:10.1126/scitranslmed.aaz4069.

Neurophysiological signatures in Alzheimer's disease are distinctly associated with TAU, amyloid-β accumulation, and cognitive decline

Kamalini G. Ranasinghe[1,*], **Jungho Cha**[1], **Leonardo Iaccarino**[1], **Leighton B. Hinkley**[2], **Alexander J. Beagle**[1], **Julie Pham**[1], **William J. Jagust**[3], **Bruce L. Miller**[1], **Katherine P. Rankin**[1], **Gil D. Rabinovici**[1,2], **Keith A. Vossel**[1,4,†], **Srikantan S. Nagarajan**[2,†]

[1]Memory and Aging Center, Department of Neurology, University of California, San Francisco, San Francisco, CA 94158, USA.

[2]Department Radiology and Biomedical Imaging, University of California, San Francisco, San Francisco, CA 94143, USA.

[3]Helen Wills Neuroscience Institute, UC Berkeley, Berkeley, CA 94720, USA.

[*]Corresponding author. kamalini.ranasinghe@ucsf.edu.

Author contributions: K.G.R., K.A.V., S.S.N., and G.D.R. designed the study, analyzed and interpreted the data, and contributed to manuscript writing. A.J.B. contributed to MEG data collection. J.P. contributed to PET data collection. K.G.R., K.A.V., A.J.B., J.P., G.D.R., B.L.M., and K.P.R. contributed to clinical data collection. J.C. and L.I. contributed to PET imaging analysis. L.B.H. contributed to MEG analysis. K.G.R., K.A.V., S.S.N., G.D.R., K.P.R., B.L.M., and W.J.J. contributed to all sections of data analysis and interpretation of findings. K.P.R., G.D.R., B.L.M., K.A.V., and K.G.R. contributed to characterization of patient cohorts.

[†]Co-senior authors.

SUPPLEMENTARY MATERIALS

stm.sciencemag.org/cgi/content/full/12/534/eaaz4069/DC1

Fig. S1. Differential patterns of resting-state neural synchronizations between AD phenotypes.
Fig. S2. TAU and Aβ depositions in AD.
Fig. S3. Global cognitive performance and dementia severity in AD cohort.
Fig. S4. TAU and Aβ depositions in normal controls.
Fig. S5. Degree of head movement in patients with AD and age-matched controls during MEG scan acquisition.
Fig. S6. Thresholding between each MEG-derived synchrony measures and PET-derived tracer uptakes.
Table S1. Neuropsychological test performance in AD variants.
Table S2. General linear model outcome with *APO*-ε4 career status included into the model to examine the associations between neural synchronization deficits and the degree of TAU and Aβ depositions.
Table S3. Mixed model analysis of associations between MMSE and frequency-specific synchrony deficits.
Table S4. Biomarkers of patients with AD.
Data file S1. Raw data.
View/request a protocol for this paper from *Bio-protocol*.

Competing interests: K.G.R., J.C., L.I., L.B.H., A.J.B., J.P., K.P.R., K.A.V., and S.S.N. declare that they have no competing interests relevant to this work. B.L.M. serves as medical director for the John Douglas French Foundation, scientific director for the Tau Consortium, director/medical advisory board of the Larry L. Hillblom Foundation, and scientific advisory board member for the National Institute for Health Research Cambridge Biomedical Research Centre. G.D.R. receives research support from Avid Radiopharmaceuticals, Eli Lilly, GE Healthcare, and Life Molecular Imaging; has served on scientific advisory boards for Axon Neurosciences, Eisai, Genentech, and Merck; and has received honoraria for speaking engagements from GE Healthcare. W.J.J. serves as a consultant to Genentech and Novartis.

Data and materials availability: All data associated with this study are present in the paper and/or in the Supplementary Materials. Unthresholded group images for frequency-specific MEGI data and average group values for flortaucipir and ^{11}C-Pib uptake are uploaded to NeuroVault (https://neurovault.org/collections/VONTMUPP/). Anonymized subject data will be shared on request from qualified investigators for the purposes of replicating procedures and results and for other noncommercial research purposes within the limits of participants' consent. Investigators will use a standard material transfer agreement for distribution of data.

Author Manuscript Author Manuscript Author Manuscript Author Manuscript

[4]N. Bud Grossman Center for Memory Research and Care, Institute for Translational Neuroscience, and Department of Neurology, University of Minnesota, Minneapolis, MN 55455, USA.

Abstract

Neural synchrony is intricately balanced in the normal resting brain but becomes altered in Alzheimer's disease (AD). To determine the neurophysiological manifestations associated with molecular biomarkers of AD neuropathology, in patients with AD, we used magnetoencephalographic imaging (MEGI) and positron emission tomography with amyloid-beta (Aβ) and TAU tracers. We found that alpha oscillations (8 to 12 Hz) were hyposynchronous in occipital and posterior temporoparietal cortices, whereas delta-theta oscillations (2 to 8 Hz) were hypersynchronous in frontal and anterior temporoparietal cortices, in patients with AD compared to age-matched controls. Regional patterns of alpha hyposynchrony were unique in each neurobehavioral phenotype of AD, whereas the regional patterns of delta-theta hypersynchrony were similar across the phenotypes. Alpha hyposynchrony strongly colocalized with TAU deposition and was modulated by the degree of TAU tracer uptake. In contrast, delta-theta hypersynchrony colocalized with both TAU and Aβ depositions and was modulated by both TAU and Aβ tracer uptake. Furthermore, alpha hyposynchrony but not delta-theta hypersynchrony was correlated with the degree of global cognitive dysfunction in patients with AD. The current study demonstrates frequency-specific neurophysiological signatures of AD pathophysiology and suggests that neurophysiological measures from MEGI are sensitive indices of network disruptions mediated by TAU and Aβ and associated cognitive decline. These findings facilitate the pursuit of novel therapeutic approaches toward normalizing network synchrony in AD.

INTRODUCTION

Alzheimer's disease (AD) is the most common cause of dementia in older adults and is characterized by progressive impairments in synapses, neural networks, and related cognitive functions (1–3). Aberrant neurophysiological manifestations in hippocampal and cortical circuits have been implicated in causing cognitive deficits in preclinical AD research where abnormally hyper- and hypo-active neurons and altered oscillatory rhythms have been linked to mechanisms mediated by amyloid-beta (Aβ) and microtubule-associated protein TAU in transgenic mouse models of AD (4–9). In patients with AD, recent positron emission tomography (PET)–based methods have transformed our understanding of AD pathophysiology. Tracers that bind to extracellular Aβ plaques and abnormally phosphorylated TAU now make it possible to visualize the origins and spread of these abnormal proteins during life (10–12). However, the aberrant neurophysiological manifestations associated with AD pathophysiology in humans remain poorly understood.

Electroencephalography (EEG) and magnetoencephalography (MEG) are two noninvasive neurophysiological modalities that are sensitive to postsynaptic current flows in neocortical pyramidal cells with high temporal resolution. In patients with AD, EEG and MEG studies have shown reduced alpha power (8 to 13 Hz) in temporal and occipital sensors and enhanced delta-theta power (2 to 8 Hz) in frontal and temporal sensors (13–15). Similarly, MEG studies in subjects with prodromal AD with positive Aβ-PET have revealed increased

Author Manuscript Author Manuscript Author Manuscript Author Manuscript

power in delta-theta bands as spectral signatures of MEG sensors associated with increased regional Aβ depositions and cellular hypometabolism (16–18). Other studies using MEG sensor data to investigate patients with AD-related dementia have reported consistent patterns of increased delta-theta in frontal and temporal sensors and decreased alpha in temporal and occipital sensors in measures of power and synchrony (14, 19, 20). Although these studies do not describe neural sources of network deficits detected in MEG and EEG sensors, they demonstrate the sensitivity of MEG and EEG to detect functional changes in early stages of AD. Because MEG can be more facilely used in conjunction with inverse algorithms that enable estimation of brain activity that contribute to observed sensor data, it can be used uniquely to examine the neuronal activations and communications across the whole brain, as well as breakdown of neural networks in neurodegenerative diseases (21). In combination with molecular imaging, MEG can help elucidate the biological bases of network deficits and their specific associations with AD pathophysiology.

Studies using functional magnetic resonance imaging (fMRI), a well-established imaging modality that measures changes in the blood oxygen level–dependent (BOLD) signal as a surrogate for neuronal activity, have demonstrated dysfunctional large-scale neural networks, most notably the default mode network (DMN), in patients with AD (22–24). Furthermore, in healthy older adults, neuroimaging studies combining fMRI with Aβ-PET and TAU-PET have identified associations between functional connectivity and the degree of Aβ and TAU deposition in the brain (25, 26). The latter studies have revealed distinctive as well as interactive effects of Aβ and TAU on network integrity. For example, cognitively healthy, Aβ-positive individuals showed increased functional connectivity within DMN at low concentrations of TAU and decreased functional connectivity at high concentrations of TAU. However, the poor temporal resolution of fMRI has limited ability to delineate the associations between precise timing of neurophysiological events and AD pathophysiology.

A better understanding of the neurophysiological signatures associated with Aβ and TAU in humans is essential to fulfill a critical gap in our understanding to link the findings of network dysfunction in animal models to those in humans. Patients with AD may present with uniquely focal neurobehavioral phenotypes reflecting dysfunction of specific neural systems. The three most predominant AD neurobehavioral phenotypes include amnestic/dysexecutive AD (AD-amnestic/dysexecutive) characterized by damage to frontal executive and medial temporal memory systems, logopenic variant of primary progressive aphasia (AD-lvPPA) with damage to language systems (27), and posterior cortical atrophy (AD-PCA) with damage to visual systems (28). The focality and system-specific neurobehavioral features do not reflect regional patterns of Aβ accumulations, but they do show strong correspondence to the regional patterns of TAU accumulations and neuronal loss. The neurophysiological abnormalities in these AD variants are not known.

In the present study, we hypothesized that, in patients with AD, frequency-specific neural oscillatory activity from distinct neural populations will be associated with explicit vulnerabilities to Aβ and TAU accumulations. We leveraged the high spatial and precise temporal resolution of MEG imaging (MEGI) to characterize network abnormalities in patients on the AD pathophysiological continuum and used a multimodal imaging approach combining MEGI, Aβ-PET, and TAU-PET. MEGI combines MEG sensor measurements

Author Manuscript Author Manuscript Author Manuscript Author Manuscript

with individualized MRI data and inverse algorithms to generate functional maps of brain activity and determines accurate neuronal sources of electrophysiological signals (29). We examined the neuronal synchrony within alpha (8 to 12 Hz) and delta-theta (2 to 8 Hz) frequency bands in patients with AD [$n = 60$ patients with probable AD or mild cognitive impairment (MCI) due to AD (30, 31); Clinical Dementia Rating (CDR) range, 0.5 to 2; Table 1] compared with age-matched controls ($n = 20$) and determined the associations between frequency-specific neuronal synchrony deficits and Aβ burden, TAU burden, and global cognitive decline. We also examined the patterns of frequency-specific neuronal synchrony deficits in each AD neurobehavioral phenotype.

RESULTS

Patients with AD exhibit hyposynchronous alpha rhythms and hypersynchronous delta-theta rhythms

The direct voxel-wise comparison of resting-state global neuronal synchrony between patients with AD and age-matched controls revealed distinct deficits within alpha (8 to 12 Hz) and delta-theta (2 to 8 Hz) frequency bands (Fig. 1). We estimated the global neuronal synchrony within each frequency band, in each participant, by calculating the MEGI-derived voxel-wise imaginary coherence (32) based on source space reconstruction algorithms and individualized head models. Imaginary coherence at each voxel indicated the average synchrony of that voxel with the rest of the brain. We found that, in patients with AD, neuronal synchrony within the alpha band was reduced (hyposynchronous) compared to controls (Fig. 1A), whereas neuronal synchrony within the delta-theta band was increased (hypersynchronous) compared to controls (Fig. 1B). Anatomically, alpha hyposynchrony was found in clusters of voxels distributed in the left inferior temporal, left posterior parietal, and bilateral occipital regions (Fig. 1A). In contrast, delta-theta hypersynchrony was found in voxel clusters that were distributed more anteriorly, including bilateral frontal cortices, bilateral posterior parietal cortices, and right temporal cortex (Fig. 1B).

Syndrome-specific spatial patterns in AD phenotypes occur in alpha hyposynchrony but not in delta-theta hypersynchrony

We determined the specific neurobehavioral phenotype for each patient in our cohort according to the diagnostic criteria for AD-lvPPA ($n = 15$) and AD-PCA ($n = 15$) and labeled those who fulfilled the criteria for probable AD but did not meet criteria for either AD-lvPPA or AD-PCA as AD-amnestic/dysexecutive ($n = 30$). Although all three variants showed similar impairments in global cognition and equivalent degree of disease severity, each AD phenotypic variant showed a characteristic profile on neuropsychological testing (table S1). When contrasted against the age-matched control group, each AD phenotype demonstrated a syndrome-specific anatomic pattern of alpha hyposynchrony (Fig. 2A). The AD-amnestic/dysexecutive group showed a focal region of alpha hyposynchrony in bilateral posterior parietooccipital cortices, whereas the AD-lvPPA group showed a left hemisphere predominant involvement of posterior temporal cortex (Fig. 2A). AD-PCA on the other hand showed bilateral occipital alpha hyposynchrony with relatively stronger deficits in the right hemisphere (Fig. 2A). In sharp contrast to alpha hyposynchrony, the anatomic patterns of delta-theta hypersynchrony were similar across the three AD phenotypes and involved

Author Manuscript Author Manuscript Author Manuscript Author Manuscript

bilateral anterior and dorsal frontal cortices and posterior parietal cortices (Fig. 2B). Patients with AD-PCA showed additional voxel clusters of delta-theta hypersynchrony over the right posterior temporal and right occipital cortices (Fig. 2B). Direct statistical comparisons between patient subgroups further highlighted the unique spatial patterns of alpha hyposynchrony and the nonspecific spatial distributions of delta-theta hypersynchrony across AD phenotypes (fig. S1). These results suggest that alpha hyposynchrony reflects the clinical heterogeneity of AD, whereas delta-theta hypersynchrony largely represents network deficits that are nonspecific across AD phenotypes.

Alpha hyposynchrony and delta-theta hypersynchrony have different spatial associations with TAU and Aβ depositions

Next, we examined the regional relationships between protein tracer uptake (the TAU tracer, flortaucipir; and the Aβ tracer, ^{11}C-PiB) and neuronal synchrony deficits (alpha hyposynchrony and delta-theta hypersynchrony) in patients with AD. The topographic patterns of flortaucipir (TAU) and ^{11}C-PiB (Aβ) uptake were consistent with previous reports with high flortaucipir retention in temporoparietal regions (10) and high ^{11}C-PIB retention in bilateral frontal posterior parietal cortices (fig. S2) (33). As the first step in the voxel-wise spatial colocalization analysis, in each patient, we identified the supratheshold voxels showing alpha hyposynchrony, delta-theta hypersynchrony, increased flortaucipir uptake, and increased ^{11}C-PiB uptake (see Materials and Methods for details). Next, we estimated the Gwet's agreement coefficient (Gwet's AC) (34) at each voxel to determine the degree of correspondence between an abnormal index read from either modality of neuroimaging (abnormally high or low synchrony or abnormally high protein tracer uptake). We found strong colocalizations between alpha hyposynchrony and flortaucipir (Gwet's AC, >0.5; $n = 12$; Fig. 3A) with an anatomic distribution of bilateral posterior and inferior temporal cortices and the left posterior parietal cortex. This anatomic distribution, especially on the left hemisphere, was consistent with the regional pattern of alpha hyposynchrony in patients with AD as shown earlier (Fig. 1A). In contrast, there was poor spatial colocalization between alpha hyposynchrony and ^{11}C-PiB uptake (Fig. 3C). Delta-theta hypersynchrony showed strong colocalizations with both increased flortaucipir and ^{11}C-PiB uptake (Gwets AC, >0.5; $n = 18$; Fig. 3, B and D). Furthermore, the spatial overlap patterns between delta-theta hypersynchrony and flortaucipir and ^{11}C-PiB uptakes looked similar and involved multiple voxel clusters over bilateral frontal posterior parietal and posterior temporal cortices (Fig. 3, B and D). These regional patterns were also consistent with the anatomic distribution of delta-theta hypersynchrony in patients with AD as shown earlier (Fig. 1B). In summary, the spatial patterns of alpha hyposynchrony selectively colocalized with flortaucipir (TAU) uptake, whereas the spatial patterns of delta-theta hypersynchrony colocalized with both flortaucipir (TAU) and ^{11}C-PiB (Aβ) uptake.

Alpha hyposynchrony and delta-theta hypersynchrony are distinctly modulated by the degree of TAU and Aβ depositions

To examine the functional relationships between neuronal synchrony deficits and Aβ and TAU depositions, we used a voxel-wise general linear model analysis on the subset of patients with all three imaging modalities: MEG, flortaucipir (TAU) PET, and ^{11}C-PiB (Aβ) PET ($n = 12$). The dependent variable in the model was the degree of abnormal synchrony

Author Manuscript Author Manuscript Author Manuscript Author Manuscript

estimated by the *Z*-normalized imaginary coherence (based on age-matched controls) at each voxel. The predictor variables of the model included the degree of flortaucipir uptake [standardized uptake value ratio (SUVR)] and the degree of ^{11}C-PiB uptake [distribution volume ratio (DVR)] for each voxel. The frequency band identity (alpha or delta-theta) and the subject identity were included into the model (see Materials and Methods for details). This voxel-wise model revealed distinct associations of alpha and delta-theta synchrony with degree of TAU and Aβ tracer uptake (Fig. 4). The degree of flortaucipir uptake negatively modulated alpha synchrony [β = −0.68; $P < 0.0001$; SE = 0.32; 95% confidence interval (CI), −1.31 to −0.05; Fig. 4, left subplot] where higher flortaucipir uptake was associated with greater hyposynchrony in alpha band. There was no main effect of ^{11}C-PiB uptake on alpha synchrony [β = 0.47; $P = 0.059$; SE = 0.35; 95% CI, −0.22 to 1.15]. In contrast, both flortaucipir and ^{11}C-PiB uptake positively modulated delta-theta synchrony [flortaucipir: β = 1.66; $P < 0.0001$; SE = 0.23; 95% CI, 1.19 to 2.12; ^{11}C-PiB: β = 1.13; $P < 0.0001$; SE = 0.25; 95%, 0.64 to 1.62]. This is also depicted in the interaction plot (Fig. 4, right subplot) where voxels with high ^{11}C-PiB and with low flortaucipir, and low ^{11}C-PiB with high flortaucipir both showed hypersynchronous delta-theta. At voxel-level interactions, a high amount of both proteins (high ^{11}C-PiB and high flortaucipir uptake) caused a net effect of reduced synchrony in delta-theta (Fig. 4, delta-theta subplot, top right corner). These findings indicate distinct effects of TAU and Aβ depositions on neural synchronizations within specific oscillatory frequencies in AD—alpha is negatively modulated by TAU regardless of Aβ, whereas delta-theta is either positively or negatively modulated by interaction of TAU and Aβ. We also reran our model after including the *APOE*-ε4 carrier status of each subject into the model. The addition of *APOE*-ε4 carrier status did not change the associations between frequency-specific neural synchronization deficits and molecular tracer uptake in patients with AD (table S2).

Alpha hyposynchrony is associated with MMSE decline

We have demonstrated that alpha hyposynchrony, in contrast to delta-theta hypersynchrony, is strongly modulated by the amount of TAU deposition as well as more tightly linked to topography of TAU deposition representing the AD phenotypic variability. Consequently, we then predicted that alpha hyposynchrony will have stronger associations with clinical decline than delta-theta hypersynchrony. We used a linear mixed model analysis to quantify the relationship between each neuronal synchrony defect and performance on the Mini-Mental State Exam (MMSE) in a cross-sectional analysis. For this analysis, we included the subset of patients with AD ($n = 26$) who were evaluated with MMSE within 30 days of MEGI. The magnitude of alpha and delta-theta synchrony was estimated in a region of interest (ROI)–based approach where the average synchrony was estimated for each patient within the ROI showing group differences when compared with age-matched controls, for each frequency band (see Materials and Methods). Using a linear mixed model, these values were modeled against MMSE, where participants were categorized into each quartile of MMSE score distribution (MMSE performance scores divided into quartiles). With observations stratified into meaningful epochs of disease severity, this analytic approach provided precise estimates of error within these categories and allowed robust detection of associations between the patterns of change. We found a significant drop in alpha synchronizations across the MMSE quartiles starting from high to low ($F = 5.44$, $P = 0.0063$; Fig. 5A and table S3). In contrast,

Author Manuscript Author Manuscript Author Manuscript Author Manuscript

there was no significant change in delta-theta synchronizations across the MMSE quartiles ($F = 0.75$, $P = 0.5281$; Fig. 5B and table S3). Collectively, these results support the premise that changes of alpha synchronizations meaningfully correlate with global cognitive deficits in patients with AD.

DISCUSSION

We demonstrated neuronal synchrony abnormalities within alpha and delta-theta oscillatory bands and their associations with Aβ deposition, TAU deposition, and cognitive decline in AD. Patients with AD showed reduced alpha synchronizations compared with age-matched controls. The alpha-hyposynchrony was (i) closely mapped onto syndrome-specific regional deficits in each neurobehavioral phenotype of AD; (ii) topographically associated with TAU deposition and not with Aβ; (iii) modulated by the degree of TAU deposition and not by Aβ; and (iv) strongly correlated with the decline in global cognition in patients with AD. In contrast, delta-theta synchronizations were increased in patients with AD compared with age-matched controls. The delta-theta hypersynchrony was (i) located in a similar distribution in all three AD phenotypes; (ii) topographically associated with both TAU and Aβ deposition; (iii) modulated by the degree of TAU depositions as well as the degree of Aβ depositions; and (iv) not associated with MMSE decline in patients with AD. A long-known conundrum in AD research is that Aβ and TAU aggregates have discrepant spatial patterns and relationships with clinical deficits (35). Distinct relationships of alpha and delta-theta with TAU and Aβ aggregates demonstrate that diverse cellular and molecular pathways that determine alpha and delta-theta frequencies may have specific vulnerabilities to AD pathophysiological mechanisms (36).

Alpha oscillations primarily deliver an overall inhibitory influence (37), where alpha power and synchrony are modulated to down-regulate the task-irrelevant information network activity while keeping a high signal-to-noise ratio within task-relevant networks (38, 39). Thus, it is conceivable that local neuronal hyperexcitability is a potential downstream effect of impaired alpha synchronizations in affected neural networks. Network hyperexcitability and aberrant neuronal firing are key findings in transgenic mouse models of AD (40). Consistent with these findings, our group previously reported a higher incidence of subclinical epileptiform activity in patients with AD than age-matched control participants (41). Both these lines of evidence support the hypothesis that intrinsic deficits of inhibitory mechanisms contribute to AD pathophysiology. The unique regional patterns of alpha hyposynchrony in each clinical phenotype of AD identified in the current study indicates the selective vulnerability of networks to develop deficits in alpha rhythms, which may subsequently contribute to characteristic cognitive defects in patients with AD. Network abnormalities occur many years before the structural deficits and overt pathological changes in AD as well as clinical symptoms (42). Future studies on prodromal and preclinical AD will determine the extent to which alpha deficits may indicate early manifestations of network abnormalities in AD.

The current study highlighted several key parallels between deficits in alpha synchrony and TAU deposition. First, there was a strong topographical relationship between alpha hyposynchrony and flortaucipir uptake. Previous neuroimaging studies have shown that TAU

Author Manuscript Author Manuscript Author Manuscript Author Manuscript

deposition has distinct anatomic relationships in each AD phenotype closely mapping to the specific neural network affected (10). Our findings of alpha hyposynchrony closely resembles the same regional heterogeneity across the three neurobehavioral AD phenotypes. Second, cognitive deficits in patients with AD are strongly correlated with TAU depositions, whereas only weakly associated with Aβ depositions (33, 43, 44). Consistent with this observation, we found that alpha synchrony was correlated with MMSE deficits in patients with AD. Third, our general linear model identified a strong main effect of flortaucipir uptake on alpha hyposynchrony but no main effect of ^{11}C-PIB uptake on alpha synchrony. Collectively, these findings indicate that impaired alpha synchrony within focal neural networks is likely an important consequence of TAU-mediated pathophysiological mechanisms in AD. Furthermore, normalizing long-range alpha synchrony may hold promise as an intriguing neuromodulatory target (45, 46). Prospective and longitudinal studies combining MEG and PET will assess the utility of regional alpha synchrony as a potential biomarker to assess therapeutic efficacy of new TAU reduction therapies in AD.

The anatomic distribution of delta-theta hypersynchrony shows a remarkable overlap with the brain regions identified as anterior and dorsal DMN. In the context of recent fMRI experiments demonstrating increased DMN connectivity, especially in the earliest stages of AD pathophysiological continuum (26, 47), delta-theta hypersynchrony may characterize the neurophysiological signatures of a functional up-regulation of network activity. Whether this increased synchrony depicts mechanisms that are compensatory or contributory to network disruption in AD remains to be uncovered. Furthermore, recent studies illustrate unique modulations of Aβ and TAU deposition on network-specific functional connectivity in humans. For example, Aβ+ healthy individuals showed increased DMN connectivity in the presence of low TAU depositions and decreased DMN connectivity in the presence of high TAU depositions (26). Our general linear model results, which demonstrated that delta-theta synchrony is strongly modulated by Aβ deposition yet being influenced by the degree of TAU deposition, are a consistent parallel with such phenomenon. For example, when TAU deposition was low, higher amounts of Aβ positively modulated delta-theta synchrony, whereas when TAU deposition was high, higher amounts of Aβ negatively modulated delta-theta synchrony. Although the sequential relationship of which of these abnormalities comes first still remains unknown, according to the amyloid-cascade hypothesis, (48, 49) it is reasonable to consider that Aβ-induced delta-theta hypersynchrony could precede, and lead to, TAU-induced hyposynchrony. Future studies in presymptomatic and prodromal AD will delineate these exact relationships. Moreover, treatment with levetiracetam as a network stabilization target in AD have demonstrated reductions in delta synchrony (50), indicating the potential benefit of this neurophysiological index as a biomarker.

The failure of clinical trials to transfer therapies from preclinical to clinical studies in AD highlights our limited knowledge of how abnormal neurophysiology in animal models reflects pathophysiological mechanisms in the human condition. Our multimodal imaging approach combining MEG, flortaucipir–^{11}C-PIB-PET uncovered key observations highly relevant to studies examining Aβ- and TAU-mediated cellular toxicity in AD transgenic mice. Increased neuronal activity and network hypersynchrony associated with higher Aβ burden are widely reported in AD transgenic mice (4, 9, 40, 51). In contrast, decreased neuronal activity and impaired network synchrony have been reported in association with the

Author Manuscript Author Manuscript Author Manuscript Author Manuscript

presence of TAU aggregation in P301L TAU transgenic mice (5). The main effects of ^{11}C-PIB-PET uptake and flortaucipir uptake from our general linear model, associated with an increased and decreased neuronal synchrony, respectively, fit nicely with these preclinical results. Furthermore, our model revealed an interaction between ^{11}C-PIB-PET uptake and flortaucipir uptake on neuronal synchrony. Many preclinical studies have reported dependencies of Aβ-mediated toxicity on TAU, with a dominating effect of TAU to impair functional integrity of neural circuits (8) as well as TAU being a mediator of *A*β toxicity in AD (52). Our results underscore that the overall neurophysiological effect of these protein-specific toxicities manifests within distinct frequency oscillatory bands—alpha being hyposynchronous, and delta-theta being hypersynchronous.

A key distinction between human and rodent data is that, whereas human resting brain rhythms are dominated by two clear peaks—the strongest created by alpha oscillations (8 to 12 Hz) and the second strongest created by delta-theta oscillations (2 to 8 Hz)—rodents show only a single predominant peak of theta oscillations (4 to 12 Hz) (53). A clear alpha peak is virtually absent during rest in mouse brain (54, 55). Despite these differences, the range of oscillatory frequencies are remarkably similar in all mammalian brains tested and range from slow oscillations of 1 to 2 Hz to fast oscillations >200 Hz (54). Furthermore, cross-species spectral similarity is also seen in sleep spindles that have the same frequency (12 to 18 Hz) and duration in both rodents and humans (56). Therefore, brain oscillations may share fundamental properties across mammals albeit with fine-tuning optimized for unique genetic, environmental, and behaviors characteristics of each individual species. Findings of widely reported theta oscillations in AD transgenic mice, as such, may potentially represent both delta-theta and alpha oscillatory bands in the human condition (9, 57, 58). The current results further emphasize the importance of fine delineation of cross-species relationships in resting oscillatory frequencies in preclinical models to facilitate better clinical translation of such findings.

Both power and synchrony of neural oscillations are key modulators of network activity. Although to compare and contrast against power and synchrony are beyond the scope of the current manuscript, it is worth emphasizing that our findings demonstrated that changes in neuronal synchrony are robust features in early AD. Consistent with these findings, in a previous report, we demonstrated that in patients with primary progressive aphasia variants, regional patterns of neuronal synchrony detected syndrome-specific effects more robustly than regional patterns of spectral power (59). Whereas oscillatory power is a first-order estimate and represents the degree of activity within neuronal populations, neuronal synchrony is a secondary estimate and represents the degree of connectivity between neuronal populations. A recent model that elegantly incorporated both power and synchrony found that synchrony within alpha band oscillations contributes to long-range connectivity between distributed regional components of canonical networks (39). It is reasonable to conclude that secondary estimates of neuronal firing such as synchrony reflect coordinated communications within and between neural networks more accurately than power estimates and, hence, provide more robust neurophysiological indices in aging as well as in AD, where network disruption is a central underlying feature.

Author Manuscript Author Manuscript Author Manuscript Author Manuscript

Synchronized oscillations play an important mechanistic role in facilitating synaptic plasticity and in shaping the functional architecture of neuronal populations. Synchronized oscillations across brain regions may facilitate temporal coordination in spiking among target neuronal populations, a process that is known to modulate synaptic plasticity (60). Consistent with this idea, impaired synaptic plasticity has been suggested as a potential contributory cause for symptomatology of several disease conditions, including schizophrenia, autism, epilepsy, as well as neurodegenerative conditions like AD and Parkinson's disease, where abnormal synchrony has been linked to cognitive deficits (61). Synchronized oscillations can also serve as a gating mechanism that modulates the excitability of target neurons, thereby shaping the functional architecture of neuronal networks (62). The modulatory role of alpha oscillations has been demonstrated where alpha synchrony down-regulates task-irrelevant information while keeping a high signal-to-noise ratio within task-relevant networks, across several cognitive tasks including visual recognition and working memory (37–39, 63–66). Similarly, delta-theta synchrony has been shown to play a central role in memory function by coordinating interactions between the hippocampus and a wider network of regions with which it communicates (67, 68). Further investigation is required to delineate the molecular and cellular manifestations of frequency-specific synchronization deficits in AD reported in our study.

Our findings should be considered in the context of the following limitations. First, although our patient cohort was strengthened by inclusion of the three main AD neurobehavioral phenotypes, our sample size for multimodal imaging (MEGI, TAU-PET, and Aβ-PET) is relatively small (18 for amyloid-PET and MEGI and 12 for TAU-PET and MEGI). Future studies with greater sample sizes including more patients across AD variants are needed to validate the generalizability of our findings. Second, our multimodal imaging combining MEGI and PET was limited to patients with AD and did not include unimpaired controls with positive Aβ-PET. Further studies including subpopulations characterizing cognitively normal individuals with positive Aβ-PET are needed to determine whether the observed relationships between neurophysiology and AD pathophysiology represent a continuum from preclinical AD to dementia. Third, our cohort of patients with AD included individuals with less common phenotypes including AD-lvPPA and AD-PCA and represented the younger early-onset AD population than the more common late-onset AD. Despite the benefit of reasonable assurance that the clinical syndrome is caused by AD pathology with minimal confound by other age-related or neurodegenerative comorbidities in the younger cohort, our findings may be less generalizable to late-onset AD. Another limitation is the known off-target binding of flortaucipir in the basal ganglia, choroid plexus, and the meninges. These off-target sources of signal are unlikely to have driven our results because the flortaucipir increases in the current study were seen in brain areas remote from off-target binding sites.

MATERIALS AND METHODS

Study design

The objective of this study was to determine frequency-specific neurophysiological manifestations associated with molecular biomarkers of AD neuropathology—Aβ and TAU

Author Manuscript Author Manuscript Author Manuscript Author Manuscript

protein depositions. In a cross-sectional observational study in patients with AD and age-matched controls, we conducted MEGI and PET imaging with Aβ-specific radiotracer ^{11}C-PIB and TAU-specific radiotracer ^{18}F-flortaucipir. Patients and age-matched controls who fulfilled the respective eligibility criteria were recruited randomly from the University of California San Francisco (UCSF) Memory and Aging Center, Alzheimer's Disease Research Center, and the community. No power analysis was performed before the study; the cohort sizes were within the range of previous experiments using MEG and PET imaging in patients with AD (10, 11, 16, 19). Preprocessing of neuroimaging data included standard automated analytic pipelines, for each imaging modality, which were agnostic to the diagnostic and demographic characteristics of the data.

Participants

A total of 60 patients with AD and 20 age-matched controls were included in this study (Table 1). All patients fulfilled the current diagnostic criteria for probable AD or MCI due to AD (30, 31). Each participant underwent a complete clinical history, physical examination, neuropsychological evaluation, and brain MRI. In addition, each participant also underwent a 10-min session of MEG recording at rest. A subset of patients (n = 12) underwent PET with both the TAU-specific radiotracer ^{18}F-flortaucipir and the Aβ-specific radiotracer ^{11}C-PIB (n = 12 patients with all three modalities of imaging: MEG, TAU-PET, and Aβ-PET). A total of 18 patients underwent PET imaging with Aβ-specific radiotracer ^{11}C-PIB (n = 18 patients with MEG and Aβ-PET; this number included the aforementioned 12 patients with all three modalities of imaging, plus 6 additional patients with MEG and Aβ-PET).

On average, the patients were mild to moderately impaired with a mean MMSE score of 20 ± 5 (MMSE range, 6 to 29; fig. S3) and a mean CDR of 0.93 ± 0.46 (CDR range, 0.5 to 2; fig, S3). Patients with AD and controls did not differ on sex, race, or education (Table 1). Clinical diagnosis for patients with AD was established by consensus in a multidisciplinary team. Fifty-three of 60 patients were positive for either CSF- or PET-derived AD biomarkers and/or subsequently confirmed via autopsy examination (table S4). The seven patients, who were not evaluated with AD biomarkers, were clinically diagnosed and showed the characteristic pattern of volume loss on structural MRI. Each patient with AD was further assigned to their specific AD neurobehavioral phenotype. Specifically, patients with AD-lvPPA (n = 15) and patients with AD-PCA (n = 15) met the diagnostic criteria for logopenic variant of primary progressive aphasia (27) and posterior cortical atrophy (28), respectively. Age-matched normal controls were recruited from the community, and the eligibility criteria included normal cognitive performance, normal MRI, and absence of neurological, psychiatric, or other major medical illnesses. In addition, we also used an amyloid negative normative dataset from the Lawrence Berkeley National Laboratory (LBNL) to estimate the normalized scores of flortaucipir and ^{11}C-PIB uptake data (n = 29 with average age of 73 ± 7.2 and n = 53 with average age of 73 ± 7.7, for ^{11}C-PIB and flortaucipir, respectively; fig. S4). Informed consent was obtained from all participants or their assigned surrogate decision makers. The study was approved by the Institutional Review Board at UCSF, LBNL, and the University of California Berkeley.

Author Manuscript Author Manuscript Author Manuscript Author Manuscript

Neuropsychological assessment

For each participant, a structured caregiver interview was used to assess the CDR scale (69). Each participant was also assessed via an MMSE and a standard battery of neuropsychological tests (70). Statistical tests comparing demographic characteristics and cognitive abilities were performed using SAS software (SAS 9.4).

Resting-state MEG data acquisition

Each subject underwent MEG recording on a whole-head bio-magnetometer system consisting of 275 axial gradiometers (MEG International Services Ltd., Coquitlam, British Columbia, Canada). Three fiducial coils including nasion, and left and right preauricular points were placed to localize the position of the head relative to the sensor array and later coregistered to each individual's respective MRI to generate an individualized head shape. Data collection was optimized to minimize within-session head movements and to keep it below 0.5 cm. Five to 10 min of continuous recording was collected from each subject while lying supine and awake with eyes closed (sampling rate, 600 Hz). We selected a 60-s (1 min) continuous segment with minimal artifacts (minimal excessive scatter at signal amplitude <10 pT), for each subject, for analysis. The study protocol required the participant to be interactive with the investigator and be awake at the beginning of the data collection. Spectral analysis of each MEGI recording and the simultaneously collected scalp EEG recordings were examined to confirm that the 60-s data epoch represented awake, eyes closed resting state for each participant. Artifact detection was confirmed by visual inspection of sensor data, and channels with excessive noise within individual subjects were removed before analysis. Both controls' and patients' data were within our specified limits of signal scatter and were not different in the degree of head movement (unpaired t test: $t = 1.5$, $P = 0.13$; means ± SD for patients, 0.32 ± 0.23 cm; controls, 0.22 ± 0.23 cm; fig. S5).

Source space reconstruction of MEG data

Tomographic reconstructions of the MEG data were generated using a head model based on each participant's structural MRI. Spatiotemporal estimates of neural sources were generated using a time-frequency–optimized adaptive spatial filtering technique implemented in the Neurodynamic Utility Toolbox for MEG (NUTMEG; http://nutmeg.berkeley.edu). Tomographic volume of source locations (voxels) was computed through an adaptive spatial filter (10-mm lead field) that weighs each location relative to the signal of the MEG sensors (29, 71). The source space reconstruction approach provided amplitude estimations at each voxel derived through the linear combination of spatial weighting matrix with the sensor data matrix (71). A high-resolution anatomical MRI was obtained for each subject (see below) and was spatially normalized to the Montreal Neurological Institute template brain using the Statistical Parametric Mapping (SPM) software (www.fil.ion.ucl.ac.uk/spm), with the resulting parameters being applied to each individual subject's source space reconstruction within the NUTMEG pipeline.

Neuronal synchrony estimation

We computed imaginary coherence between voxels, for each subject, within the frequency bands of alpha (8 to 12 Hz) and delta-theta (2 to 8 Hz). On the basis of our previous MEGI

Author Manuscript Author Manuscript Author Manuscript Author Manuscript

spectral power density analyses during resting awake state in patients with AD and age-matched controls, which showed a robust low-frequency activity within the 2 to 8 Hz window, we combined the conventional delta and theta bands and created a combined delta-theta band (2 to 8 Hz) to capture the strongest low-frequency peak. Imaginary coherence captures only the coherence that cannot be explained by volume spread (32) and is a reliable metric for resting-state functional connectivity analyses (72, 73). We then computed the global functional connectivity at each voxel as the average of the Fisher's *Z*-transformed imaginary coherence values between a given voxel (10 mm isotropic) and all other voxels in the brain. To minimize spatial frequency noise in the beamformer volumes, average and variance maps for each individual frequency band were calculated and smoothed using a Gaussian kernel with a width of 20 × 20 × 20 mm full width at half maximum (74).

PET data acquisition and image processing

Detailed descriptions of flortaucipir and PiB PET acquisition are available in previous publications (10, 11). All PET scans were acquired at LBNL on Siemens Biograph 6 Truepoint PET/CT scanner (Siemens Medical Systems) in three-dimensional acquisition mode. Flortaucipir was synthesized at the LBNL Biomedical Isotope Facility (BIF) using a GE TRACERlab FXN-Pro synthesis module with a modified protocol based on an Avid Radiopharmaceuticals protocol supplied to the facility. Participants were injected with 10 mCi of tracer and scanned in list mode 80 to 100 min after injection (4 × 5-min frames). ^{11}C-PIB was also synthesized at the LBNL BIF according to a previously published protocol (75). Beginning at the start of an injection of 15 mCi of PIB into an antecubital vein, 90 min of dynamic emission data were acquired and subsequently binned into 35 frames (4 × 15, 8 × 30, 9 × 60, 2 × 180, 10 × 300, and 2 × 600s). Flortaucipir and ^{11}C-PIB PET images were reconstructed using an ordered subset expectation maximization algorithm with weighted attenuation and smoothed with a 4-mm Gaussian kernel with scatter correction. Image resolution, calculated using a Hoffman brain phantom, was 6.5 × 6.5 × 7.25 mm^3. Ninety minutes of dynamic postinjection data for PIB and 80 to 100 min of postinjection data for flortaucipir were used for the following PET processing.

PET data were realigned and coregistered onto their corresponding T1 image using the Statistical Parametric Mapping 12 (SPM12; www.fil.ion.ucl.ac.uk/spm/). For PIB, 90-min DVR images were created using Logan graphical analysis (76), using the cerebellar gray matter as the reference region. For flortaucipir, 80- to 100-min SUVR images were created using inferior cerebellar gray matter as the reference region (77). Cerebellar gray matter and inferior cerebellar gray matter were segmented using FreeSurfer 5.3 (http://surfer.nmr.mgh.harvard.edu) (78) and inferior parcels from the spatially unbiased atlas template of the cerebellum and brainstem (79).

Spatial colocalization analysis

To determine the spatial colocalization between MEG-derived neuronal synchrony deficits and the PET-derived abnormal amounts of tracer uptakes, we determined the Gwet's AC (34) in a voxel-wise analysis. Gwet's AC is a reliable measure of interrater concordance and ranges from −1 to +1. Values >0.5 indicate high agreement between the test modalities, and values <−0.5 indicate high disagreement. Zero indicates no relationship. The Gwet's AC

Author Manuscript Author Manuscript Author Manuscript Author Manuscript

estimates the proportion of scores that are in agreement by chance and reduces bias of agreement due to chance to an appropriate magnitude (34). In our analysis, we created voxel-wise binary maps for each participants' alpha synchrony, delta-theta synchrony, flortaucipir uptake, and ^{11}C-PIB uptake. To generate binary maps for alpha synchrony and delta-theta synchrony, we first created Z scored voxel-wise images for each patient, based on the mean and SD values derived from our age-matched control cohort. To generate binary maps for flortaucipir and ^{11}C-PIB uptake data, we created age-corrected voxel-wise Z score images based on the mean and SD values derived from a normative cohort examined at the LBL. Next, we binarized each Z map (alpha, delta-theta, flortaucipir, and ^{11}C-PIB) for each patient and identified the suprathreshold voxels. To make sure that the binary images from the two modalities of imaging (MEG and PET) are at comparable degree of strength, we examined the thresholding across the full range of distribution in each modality and determined the cutoffs where the ratio between the MEG image and PET image holds equivalent strength in their binary images (fig. S6). On the basis of this analysis, we thresholded alpha synchrony maps at $Z \leq -0.25$, delta-theta synchrony maps at $Z \geq 0.25$, flortaucipir maps at $Z \geq 3.5$, and ^{11}C-PIB maps at $Z \geq 3.5$. Next, we calculated the Gwet's AC at each voxel between the binary maps for the following combinations: alpha and flortaucipir; delta-theta and ^{11}C-PIB; alpha and ^{11}C-PIB; and delta-theta and flortaucipir. The images were thresholded to depict the agreement scores ≥0.5 and ≤−0.5 representing only the voxels with high degree of agreement or high degree of disagreement.

Magnetic resonance image acquisition and analysis

Structural brain images were acquired from all participants using a unified MRI protocol on a 3-Tesla Siemens MRI scanner at the Neuroscience Imaging Center at UCSF. Structural MRIs were used to generate individualized head models for source space reconstruction of MEG sensor data. The structural MRI scans were also used in the clinical evaluations of patients with AD to identify the pattern of gray matter volume loss to support the diagnosis of AD.

Statistical analyses

Using statistical nonparametric whole-brain mapping methods incorporated in the NUTMEG toolbox (29, 71), we examined the group-level differences in global functional connectivity between patients with AD and age-matched controls. We also examined the group differences between AD phenotypes. In the latter analyses, we contrasted each AD phenotype against the pooled sample of other two phenotypic subgroups (AD-amnestic/dysexecutive versus AD-lvPPA and AD-PCA; AD-lvPPA versus pooled AD-amnestic/dysexecutive and AD-PCA; and AD-PCA versus pooled AD-amnestic/dysexecutive and AD-lvPPA). Statistical comparisons were estimated by obtaining a permuted distribution (through 2N possible combinations of negations) and estimating the significance of the test statistic (imaginary coherence) value from its position in this permuted distribution. To correct for multiple comparisons, we used 5% false discovery rate (FDR) in our analysis and thresholded the images with adjusted P values. Specifically, we determined the corrected P value threshold at the 5% FDR cutoff for all voxels that showed effects at the uncorrected $P < 0.05$ threshold. The voxels that survived the FDR correction were then further thresholded using cluster correction procedure in NUTMEG (29, 59) with a cutoff of 25 voxels (only the

Author Manuscript Author Manuscript Author Manuscript Author Manuscript

clusters with 25 congruent voxels remained), and P values thresholded to $P < 0.01$. Clusters in the thresholded statistical maps were discarded if they fell below the 95% of null-distribution cutoff after permutation testing and did not meet the required minimum value of 25 contiguous voxels at $P < 0.01$. This approach minimized the possibility of observing spurious effects.

We used a general linear model (PROC GLM in SAS) to examine the functional associations between the frequency-specific neuronal synchrony deficits and the degree of PET tracer uptake in a voxel-wise analysis. This analysis included the subset of patients ($n = 12$) who were evaluated with all three imaging modalities including MEG, flortaucipir PET, and ^{11}C-PIB PET. The independent variables include the SUVR value of flortaucipir and the DVR value of ^{11}C-PIB at each voxel. The dependent variable included the Z-normalized imaginary coherence at each voxel. We used a single general linear model with both the alpha and delta-theta frequency bands and included the frequency band identity as well as the subject identity into the model. In addition to the main effects of the degree of flortaucipir uptake and ^{11}C-PIB uptake, the model also examined the interaction between TAU and Aβ on each frequency band separately.

To examine the associations between frequency-specific neuronal synchrony abnormalities and cognitive deficits, we used a mixed model approach (PROC MIXED in SAS) (70). This analysis was performed on the subset of patients with AD ($n = 26$) who were evaluated with MMSE within 30 days of MEG. We first created masks based on the regions that were significant in the group comparison between age-matched controls and each AD phenotype, resulting in three different masks for each frequency band, one for AD-amnestic/dysexecutive, one for AD-lvPPA, and one for AD-PCA. Next, we calculated mean voxel-wise alpha synchrony and delta-theta synchrony for each patient with AD within their respective phenotype-specific mask. Next, based on the quartiles of the distribution of MMSE in our cohort of patients with AD, we categorized each patient with AD into one of four stages of MMSE depicting their global cognitive dysfunction. The four stages of MMSE identified by the quartile boundaries included 30–24, 23–22, 21–19, and 18–0. Two separate mixed models included alpha and delta-theta synchrony as dependent variables, respectively, whereas MMSE-stage consisted of the categorical predictor variables. The models were adjusted for age and sex, and the patient identity was entered as a repeated factor. When comparing between least squares means of each pairwise quantile subgroups, the values were adjusted to multiple comparisons based on Bonferroni method (critical P value threshold 0.05/6 = 0.0083). This approach allowed us to examine the relationship between the degree of neuronal synchrony and the deficits in MMSE while having equal representation of patients along the distribution of MMSE.

Supplementary Material

Refer to Web version on PubMed Central for supplementary material.

Author Manuscript Author Manuscript Author Manuscript Author Manuscript

Acknowledgments:

We would like to thank all of the study participants and their families for their generous support to our research. We would also like to acknowledge Avid Radiopharmaceuticals for enabling the use of the ^{18}F-flortaucipir tracer by providing the precursor.

Funding: This study was supported by the National Institutes of Health grants: K08AG058749 (to K.G.R.), F32AG050434-01A1 (to K.G.R.), K23 AG038357 (to K.A.V.), P50 AG023501 (to B.L.M.), P01 AG19724 (to B.L.M.), P50-AG023501 (to B.L.M. and G.D.R.), R01 AG045611 (to G.D.R.), AG034570 (to W.J.), R21 NS76171 (to S.S.N.), DC013979 (to S.S.N.), NS066654 (to S.S.N.), and NS64060 (to S.S.N.); the National Science Foundation grant BCS-1262297 (to S.S.N.); a grant from John Douglas French Alzheimer's Foundation (to K.A.V.); grants from the Larry L. Hillblom Foundation: 2015-A-034-FEL (to K.G.R.) and 2019-A-013-SUP (to K.G.R.); a grant from the Alzheimer's Association (PCTRB-13-288476) and made possible by Part the Cloud (ETAC-09-133596 to K.A.V.); a grant from Tau Consortium (to G.D.R. and W.J.J.); a gift from the S. D. Bechtel Jr. Foundation to K.A.V. and a gift from Ricoh MEG Inc to S.S.N.

REFERENCES AND NOTES

1. Selkoe DJ, Alzheimer's disease is a synaptic failure. Science 298, 789–791 (2002). [PubMed: 12399581]
2. Terry RD, Masliah E, Salmon DP, Butters N, DeTeresa R, Hill R, Hansen LA, Katzman R, Physical basis of cognitive alterations in Alzheimer's disease: Synapse loss is the major correlate of cognitive impairment. Ann. Neurol 30, 572–580 (1991). [PubMed: 1789684]
3. Alzheimer's Association, 2018 Alzheimer's disease facts and figures. Alzheimers Dement. 14, 367–425 (2018).
4. Busche MA, Eichhoff G, Adelsberger H, Abramowski D, Wiederhold K-H, Haass C, Staufenbiel M, Konnerth A, Garaschuk O, Clusters of hyperactive neurons near amyloid plaques in a mouse model of Alzheimer's disease. Science 321, 1686–1689 (2008). [PubMed: 18802001]
5. Ahnaou A, Moechars D, Raeymaekers L, Biermans R, Manyakov NV, Bottelbergs A, Wintmolders C, Van Kolen K, Van De Casteele T, Kemp JA, Drinkenburg WH, Emergence of early alterations in network oscillations and functional connectivity in a tau seeding mouse model of Alzheimer's disease pathology. Sci. Rep 7, 14189 (2017). [PubMed: 29079799]
6. Menkes-Caspi N, Yamin HG, Kellner V, Spires-Jones TL, Cohen D, Stern EA, Pathological tau disrupts ongoing network activity. Neuron 85, 959–966 (2015). [PubMed: 25704951]
7. Angulo SL, Orman R, Neymotin SA, Liu L, Buitrago L, Cepeda-Prado E, Stefanov D, Lytton WW, Stewart M, Small SA, Duff KE, Moreno H, Tau and amyloid-related pathologies in the entorhinal cortex have divergent effects in the hippocampal circuit. Neurobiol. Dis 108, 261–276 (2017). [PubMed: 28860088]
8. Busche MA, Wegmann S, Dujardin S, Commins C, Schiantarelli J, Klickstein N, Kamath TV, Carlson GA, Nelken I, Hyman BT, Tau impairs neural circuits, dominating amyloid-β effects, in Alzheimer models in vivo. Nat. Neurosci 22, 57–64 (2019). [PubMed: 30559471]
9. Palop JJ, Mucke L, Network abnormalities and interneuron dysfunction in Alzheimer disease. Nat. Rev. Neurosci 17, 777–792 (2016). [PubMed: 27829687]
10. Ossenkoppele R, Schonhaut DR, Scholl M, Lockhart SN, Ayakta N, Baker SL, O'Neil JP, Janabi M, Lazaris A, Cantwell A, Vogel J, Santos M, Miller ZA, Bettcher BM, Vossel KA, Kramer JH, Gorno-Tempini ML, Miller BL, Jagust WJ, Rabinovici GD, Tau PET patterns mirror clinical and neuroanatomical variability in Alzheimer's disease. Brain 139, 1551–1567 (2016). [PubMed: 26962052]
11. Schöll M, Lockhart SN, Schonhaut DR, O'Neil JP, Janabi M, Ossenkoppele R, Baker SL, Vogel JW, Faria J, Schwimmer HD, Rabinovici GD, Jagust WJ, PET imaging of tau deposition in the aging human brain. Neuron 89, 971–982 (2016). [PubMed: 26938442]
12. Jagust W, Imaging the evolution and pathophysiology of Alzheimer disease. Nat. Rev. Neurosci 19, 687–700 (2018). [PubMed: 30266970]
13. Osipova D, Ahveninen J, Jensen O, Ylikoski A, Pekkonen E, Altered generation of spontaneous oscillations in Alzheimer's disease. Neuroimage 27, 835–841 (2005). [PubMed: 15961323]

Author Manuscript Author Manuscript Author Manuscript Author Manuscript

14. de Haan W, Stam CJ, Jones BF, Zuiderwijk IM, van Dijk BW, Scheltens P, Resting-state oscillatory brain dynamics in Alzheimer disease. J. Clin. Neurophysiol 25, 187–193 (2008). [PubMed: 18677182]
15. Lizio R, Vecchio F, Frisoni GB, Ferri R, Rodriguez G, Babiloni C, Electroencephalographic rhythms in Alzheimer's disease. Int. J. Alzheimers Dis 2011, 927573 (2011). [PubMed: 21629714]
16. Cuésta P, Garces P, Castellanos NP, Lopez ME, Aurtenetxe S, Bajo R, Pineda-Pardo JA, Bruña R, Marin AG, Delgado M, Barabash A, Ancín I, Cabranes JA, Fernandez A, Del Pozo F, Sancho M, Marcos A, Nakamura A, Maestú F, Influence of the APOE ε4 allele and mild cognitive impairment diagnosis in the disruption of the MEG resting state functional connectivity in sources space. J. Alzheimers Dis 44, 493–505 (2015). [PubMed: 25281603]
17. Nakamura A, Cuesta P, Fernandez A, Arahata Y, Iwata K, Kuratsubo I, Bundo M, Hattori H, Sakurai T, Fukuda K, Washimi Y, Endo H, Takeda A, Diers K, Bajo R, Maestu F, Ito K, Kato T, Electromagnetic signatures of the preclinical and prodromal stages of Alzheimer's disease. Brain 141, 1470–1485 (2018). [PubMed: 29522156]
18. Nakamura A, Cuesta P, Kato T, Arahata Y, Iwata K, Yamagishi M, Kuratsubo I, Kato K, Bundo M, Diers K, Fernandez A, Maestu F, Ito K, Early functional network alterations in asymptomatic elders at risk for Alzheimer's disease. Sci. Rep 7, 6517 (2017). [PubMed: 28747760]
19. Sami S, Williams N, Hughes LE, Cope TE, Rittman T, Coyle-Gilchrist ITS, Henson RN, Rowe JB, Neurophysiological signatures of Alzheimer's disease and frontotemporal lobar degeneration: Pathology versus phenotype. Brain 141, 2500–2510 (2018). [PubMed: 30060017]
20. Stam CJ, Jones BF, Manshanden I, van Cappellen van Walsum AM, Montez T, Verbunt JP, de Munck JC, van Dijk BW, Berendse HW, Scheltens P, Magnetoencephalographic evaluation of resting-state functional connectivity in Alzheimer's disease. Neuroimage 32, 1335–1344 (2006). [PubMed: 16815039]
21. Brookes MJ, Woolrich M, Luckhoo H, Price D, Hale JR, Stephenson MC, Barnes GR, Smith SM, Morris PG, Investigating the electrophysiological basis of resting state networks using magnetoencephalography. Proc. Natl. Acad. Sci. U.S.A 108, 16783–16788 (2011). [PubMed: 21930901]
22. Greicius MD, Srivastava G, Reiss AL, Menon V, Default-mode network activity distinguishes Alzheimer's disease from healthy aging: Evidence from functional MRI. Proc. Natl. Acad. Sci. U.S.A 101, 4637–4642 (2004). [PubMed: 15070770]
23. Jones DT, Machulda MM, Vemuri P, McDade EM, Zeng G, Senjem ML, Gunter JL, Przybelski SA, Avula RT, Knopman DS, Boeve BF, Petersen RC, Jack CR Jr., Age-related changes in the default mode network are more advanced in Alzheimer disease. Neurology 77, 1524–1531 (2011). [PubMed: 21975202]
24. Rombouts SA, Damoiseaux JS, Goekoop R, Barkhof F, Scheltens P, Smith SM, Beckmann CF, Model-free group analysis shows altered BOLD FMRI networks in dementia. Hum. Brain Mapp 30, 256–266 (2009). [PubMed: 18041738]
25. Sepulcre J, Sabuncu MR, Li Q, El Fakhri G, Sperling R, Johnson KA, Tau and amyloid β proteins distinctively associate to functional network changes in the aging brain. Alzheimers Dement. 13, 1261–1269 (2017). [PubMed: 28366797]
26. Schultz AP, Chhatwal JP, Hedden T, Mormino EC, Hanseeuw BJ, Sepulcre J, Huijbers W, LaPoint M, Buckley RF, Johnson KA, Sperling RA, Phases of hyperconnectivity and hypoconnectivity in the default mode and salience networks track with amyloid and Tau in clinically normal individuals. J. Neurosci 37, 4323–4331 (2017). [PubMed: 28314821]
27. Gorno-Tempini ML, Brambati SM, Ginex V, Ogar J, Dronkers NF, Marcone A, Perani D, Garibotto V, Cappa SF, Miller BL, The logopenic/phonological variant of primary progressive aphasia. Neurology 71, 1227–1234 (2008). [PubMed: 18633132]
28. Mendez MF, Ghajarania M, Perryman KM, Posterior cortical atrophy: Clinical characteristics and differences compared to Alzheimer's disease. Dement. Geriatr. Cogn. Disord 14, 33–40 (2002). [PubMed: 12053130]
29. Dalal SS, Zumer JM, Guggisberg AG, Trumpis M, Wong DD, Sekihara K, Nagarajan SS, MEG/EEG source reconstruction, statistical evaluation, and visualization with NUTMEG. Comput. Intell. Neurosci 2011, 758973 (2011). [PubMed: 21437174]

Author Manuscript Author Manuscript Author Manuscript Author Manuscript

30. McKhann GM, Knopman DS, Chertkow H, Hyman BT, Jack CR Jr., Kawas CH, Klunk WE, Koroshetz WJ, Manly JJ, Mayeux R, Mohs RC, Morris JC, Rossor MN, Scheltens P, Carrillo MC, Thies B, Weintraub S, Phelps CH, The diagnosis of dementia due to Alzheimer's disease: Recommendations from the National Institute on Aging-Alzheimer's Association workgroups on diagnostic guidelines for Alzheimer's disease. Alzheimers Dement. 7, 263–269 (2011). [PubMed: 21514250]

31. Albert MS, DeKosky ST, Dickson D, Dubois B, Feldman HH, Fox NC, Gamst A, Holtzman DM, Jagust WJ, Petersen RC, Snyder PJ, Carrillo MC, Thies B, Phelps CH, The diagnosis of mild cognitive impairment due to Alzheimer's disease: Recommendations from the National Institute on Aging-Alzheimer's Association workgroups on diagnostic guidelines for Alzheimer's disease. Alzheimers Dement. 7, 270–279 (2011). [PubMed: 21514249]

32. Nolte G, Bai O, Wheaton L, Mari Z, Vorbach S, Hallett M, Identifying true brain interaction from EEG data using the imaginary part of coherency. Clin. Neurophysiol 115, 2292–2307 (2004). [PubMed: 15351371]

33. Lehmann M, Ghosh PM, Madison C, Laforce R Jr., Corbetta-Rastelli C, Weiner MW, Greicius MD, Seeley WW, Gorno-Tempini ML, Rosen HJ, Miller BL, Jagust WJ, Rabinovici GD, Diverging patterns of amyloid deposition and hypometabolism in clinical variants of probable Alzheimer's disease. Brain 136, 844–858 (2013). [PubMed: 23358601]

34. Gwet KL, Computing inter-rater reliability and its variance in the presence of high agreement. Br. J. Math. Stat. Psychol 61, 29–48 (2008). [PubMed: 18482474]

35. Jack CR Jr., Bennett DA, Blennow K, Carrillo MC, Dunn B, Haeberlein SB, Holtzman DM, Jagust W, Jessen F, Karlawish J, Liu E, Molinuevo JL, Montine T, Phelps C, Rankin KP, Rowe CC, Scheltens P, Siemers E, Snyder HM, Sperling R; Contributors, NIA-AA research framework: Toward a biological definition of Alzheimer's disease. Alzheimers Dement. 14, 535–562 (2018). [PubMed: 29653606]

36. Wang X-J, Neurophysiological and computational principles of cortical rhythms in cognition. Physiol. Rev 90, 1195–1268 (2010). [PubMed: 20664082]

37. Hyafil A, Giraud AL, Fontolan L, Gutkin B, Neural cross-frequency coupling: Connecting architectures, mechanisms, and functions. Trends Neurosci. 38, 725–740 (2015). [PubMed: 26549886]

38. Lobier M, Palva JM, Palva S, High-alpha band synchronization across frontal, parietal and visual cortex mediates behavioral and neuronal effects of visuospatial attention. Neuroimage 165, 222–237 (2018). [PubMed: 29074278]

39. Sadaghiani S, Kleinschmidt A, Brain networks and α-oscillations: Structural and functional foundations of cognitive control. Trends Cogn. Sci 20, 805–817 (2016). [PubMed: 27707588]

40. Palop JJ, Chin J, Roberson ED, Wang J, Thwin MT, Bien-Ly N, Yoo J, Ho KO, Yu GQ, Kreitzer A, Finkbeiner S, Noebels JL, Mucke L, Aberrant excitatory neuronal activity and compensatory remodeling of inhibitory hippocampal circuits in mouse models of Alzheimer's disease. Neuron 55, 697–711 (2007). [PubMed: 17785178]

41. Vossel KA, Ranasinghe KG, Beagle AJ, Mizuiri D, Honma SM, Dowling AF, Darwish SM, Van Berlo V, Barnes DE, Mantle M, Karydas AM, Coppola G, Roberson ED, Miller BL, Garcia PA, Kirsch HE, Mucke L, Nagarajan SS, Incidence and impact of subclinical epileptiform activity in Alzheimer's disease. Ann. Neurol 80, 858–870 (2016). [PubMed: 27696483]

42. Mondadori CR, Buchmann A, Mustovic H, Schmidt CF, Boesiger P, Nitsch RM, Hock C, Streffer J, Henke K, Enhanced brain activity may precede the diagnosis of Alzheimer's disease by 30 years. Brain 129, 2908–2922 (2006). [PubMed: 17012294]

43. Bejanin A, Schonhaut DR, La Joie R, Kramer JH, Baker SL, Sosa N, Ayakta N, Cantwell A, Janabi M, Lauriola M, O'Neil JP, Gorno-Tempini ML, Miller ZA, Rosen HJ, Miller BL, Jagust WJ, Rabinovici GD, Tau pathology and neurodegeneration contribute to cognitive impairment in Alzheimer's disease. Brain 140, 3286–3300 (2017). [PubMed: 29053874]

44. Arriagada PV, Growdon JH, Hedley-Whyte ET, Hyman BT, Neurofibrillary tangles but not senile plaques parallel duration and severity of Alzheimer's disease. Neurology 42, 631–639 (1992). [PubMed: 1549228]

Author Manuscript Author Manuscript Author Manuscript Author Manuscript

45. Plewnia C, Rilk AJ, Soekadar SR, Arfeller C, Huber HS, Sauseng P, Hummel F, Gerloff C, Enhancement of long-range EEG coherence by synchronous bifocal transcranial magnetic stimulation. Eur. J. Neurosci 27, 1577–1583 (2008). [PubMed: 18336566]
46. Thut G, Miniussi C, New insights into rhythmic brain activity from TMS-EEG studies. Trends Cogn. Sci 13, 182–189 (2009). [PubMed: 19286414]
47. Jones DT, Knopman DS, Gunter JL, Graff-Radford J, Vemuri P, Boeve BF, Petersen RC, Weiner MW, Jack CR Jr.; Alzheimer's Disease Neuroimaging Initiative, Cascading network failure across the Alzheimer's disease spectrum. Brain 139, 547–562 (2016). [PubMed: 26586695]
48. Hardy J, Selkoe DJ, The amyloid hypothesis of Alzheimer's disease: Progress and problems on the road to therapeutics. Science 297, 353–356 (2002). [PubMed: 12130773]
49. Hardy JA, Higgins GA, Alzheimer's disease: The amyloid cascade hypothesis. Science 256, 184–185 (1992). [PubMed: 1566067]
50. Musaeus CS, Shafi MM, Santarnecchi E, Herman ST, Press DZ, Levetiracetam alters oscillatory connectivity in Alzheimer's Disease. J. Alzheimers Dis 58, 1065–1076 (2017). [PubMed: 28527204]
51. Harris JA, Devidze N, Verret L, Ho K, Halabisky B, Thwin MT, Kim D, Hamto P, Lo I, Yu G-Q, Palop JJ, Masliah E, Mucke L, Transsynaptic progression of amyloid-β-induced neuronal dysfunction within the entorhinal-hippocampal network. Neuron 68, 428–441 (2010). [PubMed: 21040845]
52. Miller EC, Teravskis PJ, Dummer BW, Zhao X, Huganir RL, Liao D, Tau phosphorylation and tau mislocalization mediate soluble Aβ oligomer-induced AMPA glutamate receptor signaling deficits. Eur. J. Neurosci 39, 1214–1224 (2014). [PubMed: 24713000]
53. Buzsáki G, Watson BO, Brain rhythms and neural syntax: Implications for efficient coding of cognitive content and neuropsychiatric disease. Dialogues Clin. Neurosci 14, 345–367 (2012). [PubMed: 23393413]
54. Buzsaki G, Rhythms of the Brain (Oxford Univ. Press, 2011).
55. Jing W, Wang Y, Fang G, Chen M, Xue M, Guo D, Yao D, Xia Y, EEG bands of wakeful rest, slow-wave and rapid-eye-movement sleep at different brain areas in rats. Front. Comput. Neurosci 10, 79 (2016). [PubMed: 27536231]
56. Sirota A, Csicsvari J, Buhl D, Buzsáki G, Communication between neocortex and hippocampus during sleep in rodents. Proc. Natl. Acad. Sci. U.S.A 100, 2065–2069 (2003). [PubMed: 12576550]
57. Mondragón-Rodriguez S, Gu N, Manseau F, Williams S, Alzheimer's transgenic model is characterized by very early brain network alterations and β-CTF fragment accumulation: Reversal by β-secretase inhibition. Front. Cell. Neurosci 12, 121 (2018). [PubMed: 29867356]
58. Das M, Maeda S, Hu B, Yu G-Q, Guo W, Lopez I, Yu X, Tai C, Wang X, Mucke L, Neuronal levels and sequence of tau modulate the power of brain rhythms. Neurobiol. Dis 117, 181–188 (2018). [PubMed: 29859869]
59. Ranasinghe KG, Hinkley LB, Beagle AJ, Mizuiri D, Honma SM, Welch AE, Hubbard I, Mandelli ML, Miller ZA, Garrett C, La A, Boxer AL, Houde JF, Miller BL, Vossel KA, Gorno-Tempini ML, Nagarajan SS, Distinct spatiotemporal patterns of neuronal functional connectivity in primary progressive aphasia variants. Brain 140, 2737–2751 (2017). [PubMed: 28969381]
60. Fries P, A mechanism for cognitive dynamics: Neuronal communication through neuronal coherence. Trends Cogn. Sci 9, 474–480 (2005). [PubMed: 16150631]
61. Uhlhaas PJ, Singer W, Neural synchrony in brain disorders: Relevance for cognitive dysfunctions and pathophysiology. Neuron 52, 155–168 (2006). [PubMed: 17015233]
62. Klimesch W, Sauseng P, Hanslmayr S, EEG alpha oscillations: The inhibition-timing hypothesis. Brain Res. Rev 53, 63–88 (2007). [PubMed: 16887192]
63. Palva S, Palva JM, Functional roles of alpha-band phase synchronization in local and large-scale cortical networks. Front. Psychol 2, 204 (2011). [PubMed: 21922012]
64. Sauseng P, Klimesch W, Doppelmayr M, Pecherstorfer T, Freunberger R, Hanslmayr S, EEG alpha synchronization and functional coupling during top-down processing in a working memory task. Hum. Brain Mapp 26, 148–155 (2005). [PubMed: 15929084]

Author Manuscript Author Manuscript Author Manuscript Author Manuscript

65. Freunberger R, Klimesch W, Griesmayr B, Sauseng P, Gruber W, Alpha phase coupling reflects object recognition. Neuroimage 42, 928–935 (2008). [PubMed: 18595738]
66. Doesburg SM, Green JJ, McDonald JJ, Ward LM, Rhythms of consciousness: Binocular rivalry reveals large-scale oscillatory network dynamics mediating visual perception. PLOS ONE 4, e6142 (2009). [PubMed: 19582165]
67. Backus AR, Schoffelen J-M, Szebényi S, Hanslmayr S, Doeller CF, Hippocampalprefrontal theta oscillations support memory integration. Curr. Biol 26, 450–457 (2016). [PubMed: 26832442]
68. Clouter A, Shapiro KL, Hanslmayr S, Theta phase synchronization is the glue that binds human associative memory. Curr. Biol 27, 3143–3148.e6 (2017). [PubMed: 28988860]
69. Morris JC, The Clinical Dementia Rating (CDR): Current version and scoring rules. Neurology 43, 2412–2414 (1993).
70. Ranasinghe KG, Rankin KP, Lobach IV, Kramer JH, Sturm VE, Bettcher BM, Possin K, Christine You S, Lamarre AK, Shany-Ur T, Stephens ML, Perry DC, Lee SE, Miller ZA, Gorno-Tempini ML, Rosen HJ, Boxer A, Seeley WW, Rabinovici GD, Vossel KA, Miller BL, Cognition and neuropsychiatry in behavioral variant frontotemporal dementia by disease stage. Neurology 86, 600–610 (2016). [PubMed: 26802093]
71. Dalal SS, Guggisberg AG, Edwards E, Sekihara K, Findlay AM, Canolty RT, Berger MS, Knight RT, Barbaro NM, Kirsch HE, Nagarajan SS, Five-dimensional neuroimaging: Localization of the time-frequency dynamics of cortical activity. Neuroimage 40, 1686–1700 (2008). [PubMed: 18356081]
72. Guggisberg AG, Honma SM, Findlay AM, Dalal SS, Kirsch HE, Berger MS, Nagarajan SS, Mapping functional connectivity in patients with brain lesions. Ann. Neurol 63, 193–203 (2008). [PubMed: 17894381]
73. Hinkley LBN, Vinogradov S, Guggisberg AG, Fisher M, Findlay AM, Nagarajan SS, Clinical symptoms and alpha band resting-state functional connectivity imaging in patients with schizophrenia: Implications for novel approaches to treatment. Biol. Psychiatry 70, 1134–1142 (2011). [PubMed: 21861988]
74. Barnes GR, Hillebrand A, Fawcett IP, Singh KD, Realistic spatial sampling for MEG beamformer images. Hum. Brain Mapp 23, 120–127 (2004). [PubMed: 15340934]
75. Mathis CA, Wang Y, Holt DP, Huang G-F, Debnath ML, Klunk WE, Synthesis and evaluation of ^{11}C-labeled 6-substituted 2-arylbenzothiazoles as amyloid imaging agents. J. Med. Chem 46, 2740–2754 (2003). [PubMed: 12801237]
76. Logan J, Fowler JS, Volkow ND, Wang GJ, Ding YS, Alexoff DL, Distribution volume ratios without blood sampling from graphical analysis of PET data. J. Cereb. Blood Flow Metab 16, 834–840 (1996). [PubMed: 8784228]
77. Baker SL, Maass A, Jagust WJ, Considerations and code for partial volume correcting [^{18}F]-AV-1451 tau PET data. Data Brief 15, 648–657 (2017). [PubMed: 29124088]
78. Fischl B, Salat DH, Busa E, Albert M, Dieterich M, Haselgrove C, van der Kouwe A, Killiany R, Kennedy D, Klaveness S, Montillo A, Makris N, Rosen B, Dale AM, Whole brain segmentation: Automated labeling of neuroanatomical structures in the human brain. Neuron 33, 341–355 (2002). [PubMed: 11832223]
79. Diedrichsen J, A spatially unbiased atlas template of the human cerebellum. Neuroimage 33, 127–138 (2006). [PubMed: 16904911]

Author Manuscript Author Manuscript Author Manuscript Author Manuscript

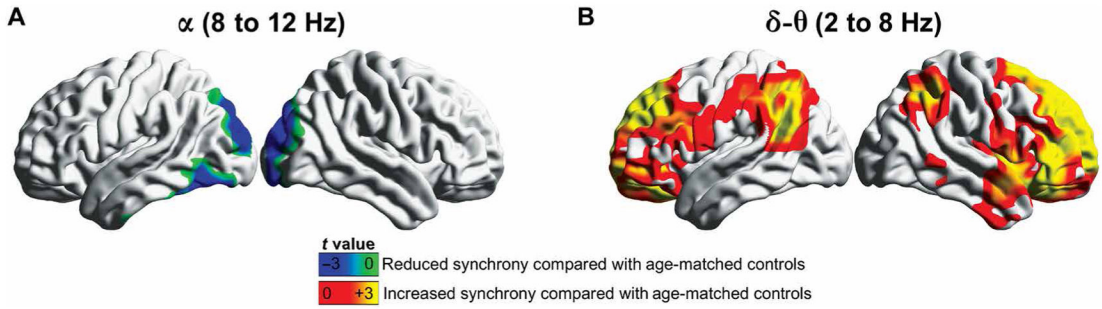

Fig. 1. Resting-state neural synchronizations in patients with AD compared with age-matched controls.

Each brain rendering depicts the *t* maps from the voxel-wise comparison of global imaginary coherence between groups for alpha (**A**) and delta-theta (**B**) oscillations. Cold colors indicate hyposynchrony, and hot colors indicate hypersynchrony. The color maps are thresholded with a cluster correction of 25 voxels ($P < 0.01$) and at 5% FDR ($n = 60$, patients with AD; $n = 20$, age-matched controls).

Author Manuscript Author Manuscript Author Manuscript Author Manuscript

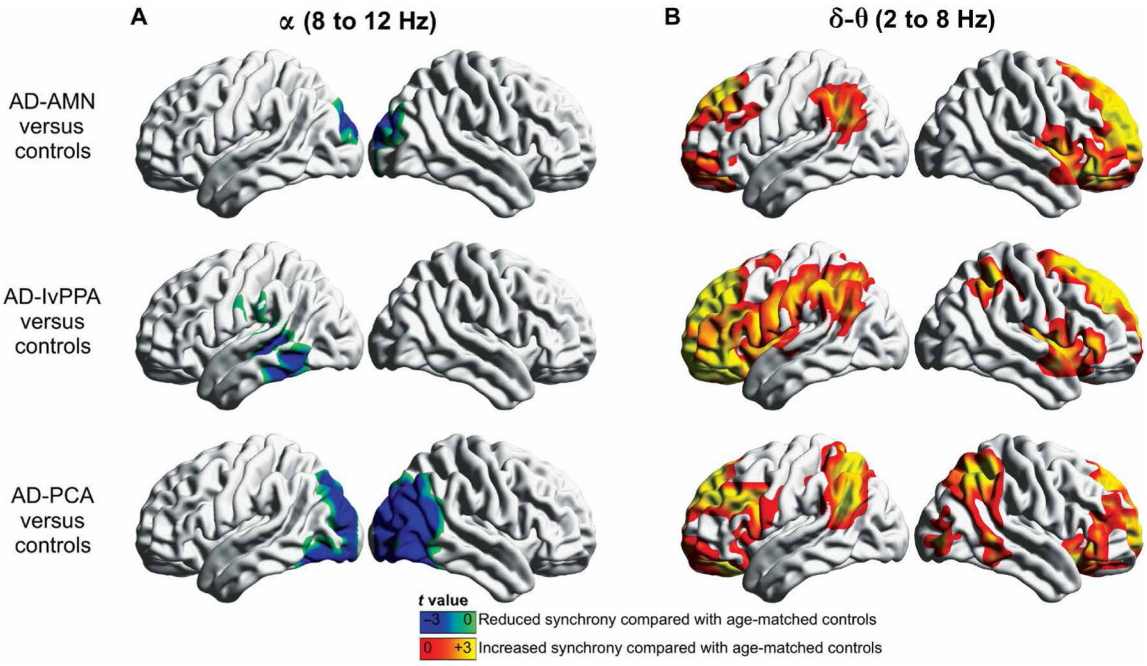

Fig. 2. Resting-state neural synchronizations in each neurobehavioral phenotype of AD compared with age-matched controls.

Each row represents the three AD phenotypes, from top to bottom, AD-amnestic/dysexecutive (AD-AMN), logopenic variant of primary progressive aphasia (AD-lvPPA), and posterior cortical atrophy (AD-PCA). The left column (**A**) shows the alpha synchrony, and the right column (**B**) shows the delta-theta synchrony, in each AD phenotype when compared with age-matched controls. Cold colors indicate hyposynchrony, and hot colors indicate hypersynchrony. The brain renderings depict the *t* maps from the voxel-wise comparison of global imaginary coherence. The color maps are thresholded with a cluster correction of 25 voxels ($P < 0.01$) at 5% FDR ($n = 30$, 15, 15, and 20 for AD-AMN, AD-lvPPA, AD-PCA, and age-matched controls, respectively).

Author Manuscript Author Manuscript Author Manuscript Author Manuscript

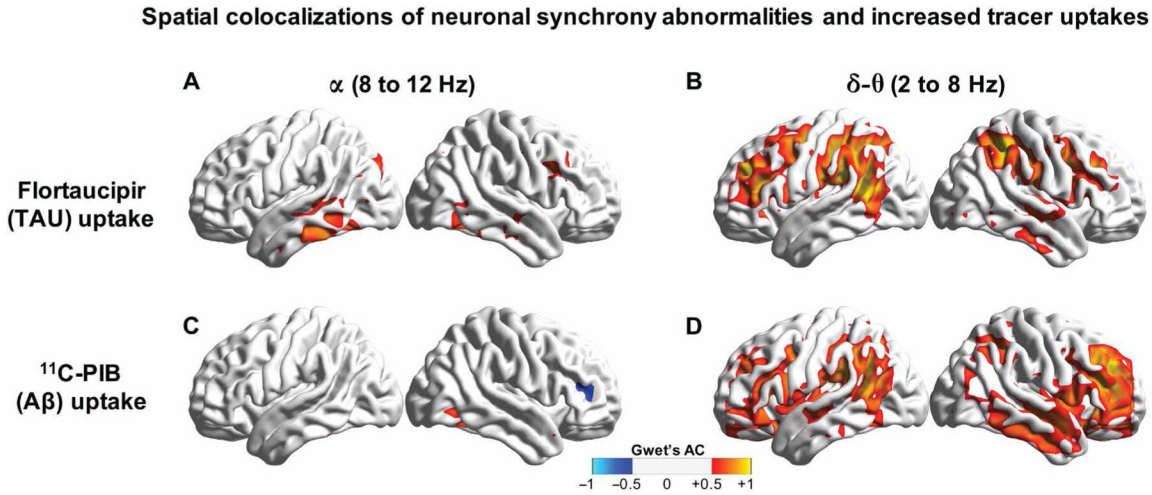

Fig. 3. Spatial colocalization between neuronal synchrony and flortaucipir and ^{11}C-PIB uptakes.

Images show the voxel-wise Gwet's Agreement coefficient (Gwet's AC) between alpha hyposynchrony and flortaucipir uptake (**A**), between delta-theta hypersynchrony and flortaucipir uptake (**B**), between alpha hyposynchrony and ^{11}C-PIB uptake (**C**), and between delta-theta hypersynchrony and ^{11}C-PIB uptake (**D**). Images are thresholded to show Gwet's AC scores depicting high agreement (>0.5; depicted in yellow-orange color scheme) or high disagreement (<−0.5; depicted in blue color scheme) [n = 12 patients included in the analyses for subplots (A) and (B); n = 18 patients included in the analyses for subplots (C) and (D)].

Author Manuscript Author Manuscript Author Manuscript Author Manuscript

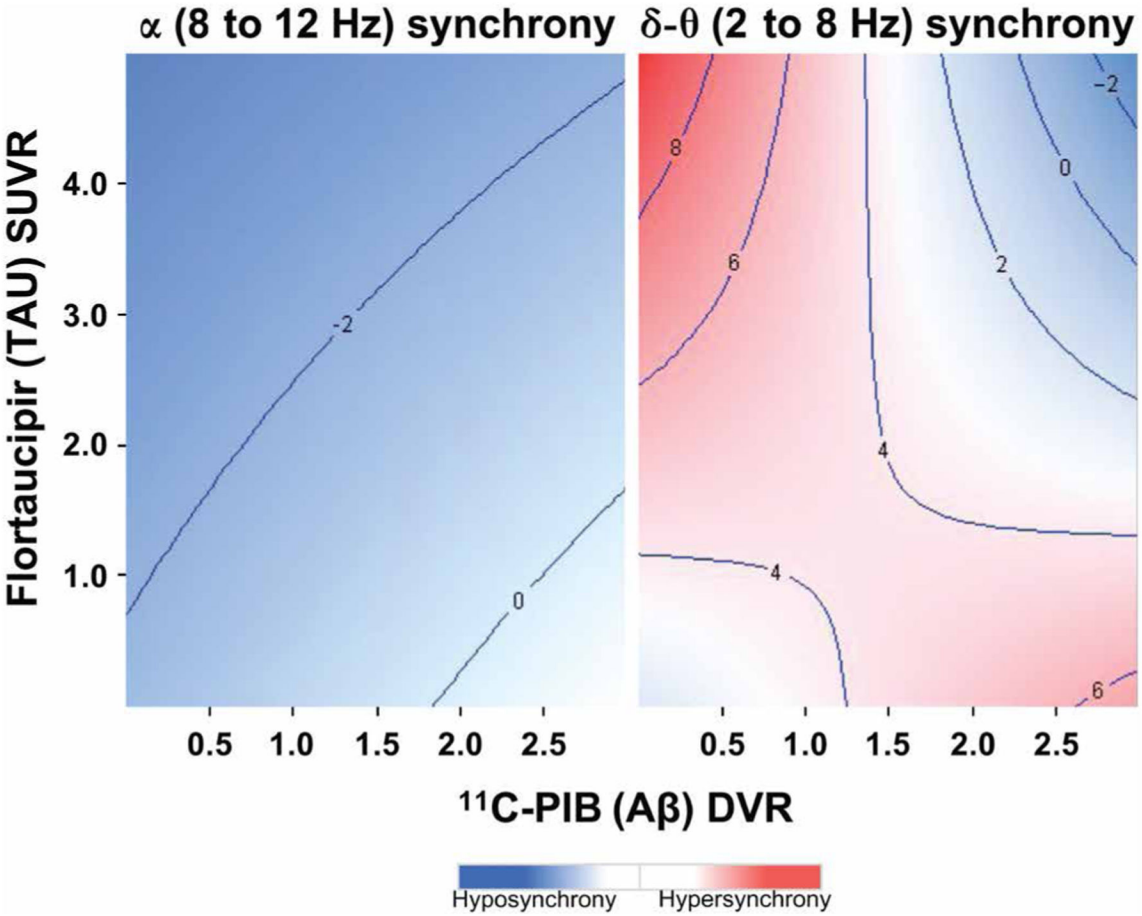

Fig. 4. Functional associations between neural synchronization deficits and the degree of Aβ and TAU depositions.

Contour plots depict the main effects and interactive effects of flortaucipir (TAU) uptake and ^{11}C-PIB (Aβ) uptake on alpha (left subplot) and delta-theta (right subplot) synchrony abnormalities in a voxel-wise general linear model based on subjects scanned with all three modalities of imaging: MEGI; flortaucipir; ^{11}C-PIB PET. *X* axes represent the degree of ^{11}C-PIB uptake (DVR), and *Y* axes represent the degree of flortaucipir uptake (SUVR). Color gradients represent the degree of neuronal synchrony represented as *Z* scores (depicted in contour lines), where blue represents reduced neuronal synchrony (hyposynchrony) and red represents increased neuronal synchrony (hypersynchrony), based on age-matched normal controls. (n = 12 patients with AD).

Author Manuscript Author Manuscript Author Manuscript Author Manuscript

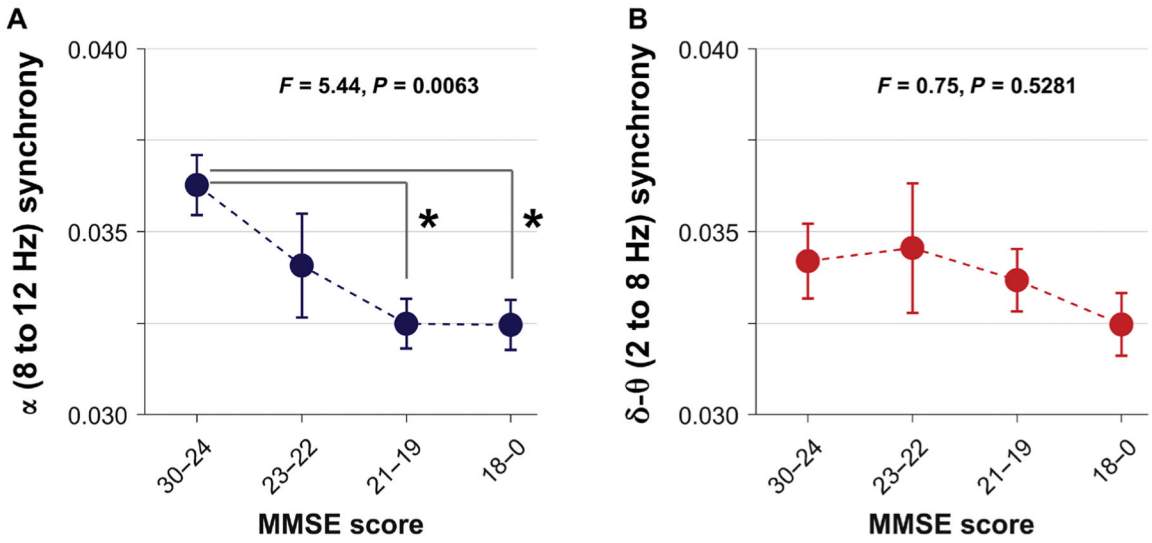

Fig. 5. Alpha synchronizations demonstrate associations with global cognitive decline in patients with AD.

Alpha (**A**) and delta-theta (**B**) synchrony is plotted against Mini Mental State Exam (MMSE) scores in patients with AD. The *X* axes show the four quartiles of MMSE. The plots depict the least square means corrected for age and sex, and the SEs, derived from the mixed model analysis. *Y* axes depict the frequency-specific neuronal synchrony values derived as global imaginary coherence (see Materials and Methods) for alpha and delta-theta bands ($n = 26$ patients with AD with MMSE evaluation within 30 days of MEGI). MMSE scores range from 0 to 30, with higher scores denoting better cognitive function.

Author Manuscript

Author Manuscript

Author Manuscript

Author Manuscript

Table 1.

Participant demographics.

	AD (*n* = 60)	Controls (*n* = 20)	*P*
Age, years	61.2 ± 7.8	64.3 ± 4.6	0.10
Female sex, no. (%)	39 (65.0)	12 (60.0)	0.69
Right handedness, no. (%)	49 (81.7)	16 (80.0)	0.25
White race, no. (%)*	54 (96.4)	18 (94.7)	0.43
Education, years	16.0 ± 2.7	17.3 ± 2.0	0.07
APOE-ε4 carrier (%)†	27 (48.2)	5 (20.8)	0.02
MMSE‡	20.4 ± 5.3	29.6 ± 0.7	<0.0001
CDR§	0.9 ± 0.5	0 ± 0	<0.0001

Values for age and education indicate means ± SD of the participants at the time of evaluation. Statistical comparisons of gender and handedness were performed using Fisher's exact test, whereas the statistical comparison of race was performed using chi-square test. Statistical comparisons of age and education were performed using unpaired *t* test.

*Race was self-reported, and the total number of observations reported for each group included $n = 56$ and $n = 19$ for patients with AD and control groups, respectively.

†Four patients with AD did not take part in the genetic analyses due to subject preferences.

‡Scores on the MMSE range from 0 to 30, with higher scores denoting better cognitive function.

§Scores on the CDR range from 0 to 3, with higher scores denoting greater impairment.